Deletion of two-component system QseBC weakened virulence of *Glaesserella parasuis* in a murine acute infection model and adhesion to host cells

Xuefeng Yan [Equal first author, 1] , **Ke Dai** [Equal first author, 2] , **Congwei Gu** [1] , **Zehui Yu** [1] , **Manli He** [1] , **Wudian Xiao** [1] , **Mingde Zhao** [1] , **LVqin He** [Corresp. 1]

[1] southwest medical university, luzhou, china

[2] Sichuan Agricultural University, chengdu, China

Corresponding Author: LVqin He
Email address: 1176044269@qq.com

The widespread two-component system (TCS) QseBC involves vital virulence regulators in *Enterobacteriaceae* and *Pasteurellaceae* . Here we studied the function of QseBC in *Glaesserella parasuis*. A Δ*qseBC* mutant was constructed using a *Glaesserella parasuis* serovar 11 clinical strain SC1401 by natural transformation. Immunofluorescence technique was used to evaluate cellular adhesion, the levels of inflammation and apoptosis. The ability of Δ*qseBC* and Δ*qseC* mutant strains to adhere to PAM and MLE-12 cells was significantly reduced. Additionally, by focusing on the clinical signs, H&E, and IFA for inflammation and apoptosis, we found that the Δ*qseBC* mutant weakened virulence in the murine models. Together, these findings suggest that QseBC plays an important role in the virulence of *Glaesserella parasuis*.

1   **Deletion of two-component system QseBC weakened virulence of *Glaesserella parasuis* in**

2   **a murine acute infection model and adhesion to host cells**

5   Xuefeng Yan[a,1], Ke dai[b,1], Congwei Gu[c], Zehui Yu[c], Manli He[c], Wudian Xiao[c], Mingde Zhao[c],

6   Lvqin He[c]*

8   [a]School of physical education, Southwest Medical University, Luzhou, China;

9   [b]Research Center of Swine Disease, College of Veterinary Medicine, Sichuan Agricultural

10   University, Chengdu 611130, China;

11   [c]Experimental animal center, Technology Department, Southwest Medical University, Luzhou,

12   China.

14   [1]Xuefeng Yan, Ke dai contributed equally to this work

15   Corresponding Author: Lvqin He, helvqin617@163.com

16   No. 1, Section 1, Xianglin Road, Southwest Medical University, Luzhou City, Sichuan Province,

17   China

31 **Abstract**

32 The widespread two-component system (TCS) QseBC involves vital virulence regulators in

33 *Enterobacteriaceae* and *Pasteurellaceae*. Here we studied the function of QseBC in *Glaesserella*

34 *parasuis*. A Δ*qseBC* mutant was constructed using a *Glaesserella parasuis* serovar 11 clinical

35 strain SC1401 by natural transformation. Immunofluorescence technique was used to evaluate

36 cellular adhesion, the levels of inflammation and apoptosis. The ability of Δ*qseBC* and Δ*qseC*

37 mutant strains to adhere to PAM and MLE-12 cells was significantly reduced. Additionally, by

38 focusing on the clinical signs, H&E, and IFA for inflammation and apoptosis, we found that the

39 Δ*qseBC* mutant weakened virulence in the murine models. Together, these findings suggest that

40 QseBC plays an important role in the virulence of *Glaesserella parasuis*.

41 **Keywords:** *Glaesserella parasuis*, TCS, Quorum sensing, QseBC, adherence, virulence

42 **1. Introduction**

43 *Glaesserella parasuis* is an opportunistic pathogen, which causes Glässer's disease (GD),

44 characterized by polyserositis, meningitis and arthritis, and has incurred significant economic

45 losses in pig industries across many countries (Oliveira and Pijoan, 2004). To date, more than 15

46 serotypes have been found for this species (Kielstein and Rappgabrielson, 1992). It is difficult to

47 prevent this disease by immunization of inactivated vaccines due to the lack of cross-protection

48 among the different serotypes of *G. parasuis* (Dai et al., 2019b). Therefore, it is critical to elucidate

49 the mechanism of *G. parasuis* survival and infection in the host for effective protective vaccine

50 research.

51 *Glaesserella parasuis* encounters varying environmental stresses during its invasion process,

52 which are vital for colonization and infection in the host (Huang et al., 2016; Hughes et al., 2009).

53 Biofilms protect bacteria from elimination by the host immune system, which can enhance

54 resistance of the bacteria to antibiotics and allow the exchange of genetic materials. Biofilms are

55 considered to be the basis of many persistent chronic infections and the cause of repeated episodes

56 of acute infection (Kaplan and Mulks, 2005; Mah, 2012). Biofilm positive strains of *G. parasuis*

57 had positive correlation with resistance to β-lactams antibiotics (Zhang et al., 2014). Therefore,

58 antibiotic resistance and biofilm-associated tolerance are important factors to consider in treating

59 *G. parasuis* infections.

60   Quorum sensing (QS) is deemed as a special ''language'' for bacteria-bacteria communication

61 in most bacteria such as *Vibrio fisheri, Pseudomonas aeruginosa*, etc (Sperandio et al., 2003).

62 QseBC, a density-sensing regulator, plays an important role in the virulence of *Enterobacteriaceae*

63 and *Pasteurellaceae* (Weigel and Demuth, 2016). Deletion of *qseC* in *Escherichia coli* and

64 UroPathogenic *E. coli* leads to aberrant activation of QseB (Kostakioti et al., 2009). QseBC plays

65 a vital role in the intracellular virulence of *Edwardsiella tarda* and *Actinobacillus*

66 *pleuropneumoniae* (Liu et al., 2015; Wang et al., 2011). QseC is important for biofilm formation

67 in *Aggregatibacter actinomycetemcomitans*, non-typeable *Haemophilus influenzae* and

68 *Salmonella enterica* serovar Typhi (Ji et al., 2017; Juarez-Rodriguez et al., 2013; Unal et al., 2012).

69 In mice infected with *Salmonella* serovar Typhimurium, deletion of *qseC* attenuated invasion of

70 epithelial cells and systemic infections, and impaired survival within macrophages (Bearson and

71 Bearson, 2008; Moreira et al., 2010). However, the mechanism of QseB phosphorylation that

72 regulates downstream genes requires further investigation.

73   In our previous studies, we found that CheY (QseB) plays vital roles in the growth and

74 colonization of *G. parasuis*. QseC weakens the tolerance to stresses such as osmotic pressure,

75 oxidative stress and heat shock. However, it was unclear whether QseBC was related to the

76 bacterial virulence in vivo. In this study, we deleted the *qseB* and *qseC* genes in the wild-type

77 strain of *G. parasuis* SC1401 and evaluated their abilities to adhere and invade cells. In addition,

78 we also evaluated the reactive oxygen species inducing ability and inflammation/apoptosis levels

79 in the murine models to analyze the virulence of the Δ*qseBC* mutant strain. This study aims to

80 verify the role of QseBC and *G. parasuis* in the virulence of animals, which contributes to better

81 understanding of the function of the two-component system and the mechanism that determines

82   the virulence level of *G. parasuis*.

83   2. Materials and Methods

84   2.1 Animals and Ethics Statement

85   Female BALB/c mice (6-week-old) were purchased from Chengdu Dossy Experimental Animal

86   Co., Ltd (Sichuan, China). The animal experiments were conducted in strict accordance with the

87   recommendations in the China Regulations for the Administration of Affairs Concerning

88   Experimental Animals (1988) and had been approved by the Institutional Animal Care and Use

89   Committee of Southwest Medical University (Approval Number 20211017-001), Lu zhou, China.

90   We did our best to provide maximum comfort and minimal stress for the mice.

91   2.2 Bacteria strains, plasmids and culture conditions

92   Bacteria strains and plasmids employed in this study are listed in Table 1. *Escherichia coli*

93   DH5α (Biomed, Beijing, China) was cultured in liquid Lysogeny Broth (LB, Difco, USA) medium

94   or on LB agar (Invitrogen, Shanghai, China) plates. *Glaesserella parasuis* strain SC1401 and its

95   derivatives were grown in tryptic soy broth (TSB; Difco, NJ, USA) or on tryptic soy agar (TSA;

96   Difco, USA) supplemented with 0.001% nicotinamide adenine dinucleotide (NAD; Sigma-

97   Aldrich, USA) and 5% inactivated bovine serum (Solarbio, Beijing, China). When required, the

98   medium was supplemented with kanamycin (kan; 100 μg/mL) or gentamicin (50 μg/mL).

99   Table 1 Bacteria strains and plasmids used in this study.

100   2.3 Construction and complementation of the *qseBC* mutant

101   The Δ*qseBC* strain and genetically complemented strains were constructed by natural

102   transformation. Naturally competent bacteria are able to take up DNA fragments from the

103   environment into their cytoplasm, and these foreign DNA fragments provide the bacteria with a

104   source of nucleic acid (Patrick and Melanie, 2013). This transformation method is the third parallel

105   gene transfer (HGT) mode, which is different from phage transduction and combined transfer, and

106   is called natural transformation.

107   To construct an in-frame nonpolar *qseBC* mutant strain of *G. parasuis*, the target vector pLQ4

108   was built as follows: the upstream (958 bp) and downstream (947 bp) fragments of the in-situ *qseB*

109   and *qseC* genes were amplified using primers P1+P2 (*qseBC*-Up-F/R, Table 2) and P3+P4 from

110   the genomic DNA of SC1401. The *qseB* and *qseC* genes have a 14 bp overlap in *G. parasuis*. The

111   kanamycin resistance cassette (935 bp) was amplified from pKD4 using primers P7+P8 (Kan-F/R).

112   The three PCR fragments were integrated by overlap PCR with primers P1+P4 (*qseBC*-Up-

113   F/*qseBC*-Down-R). The fusion segment was inserted into pk18mobsacB at the BamHI and HindIII

114   sites to generate the recombinant plasmid pLQ4. Finally, the resulting plasmid pLQ4 was

115   transformed into SC1401 using a natural transformation technique. Transformant bacteria were

116   incubated at 37°C for 36 h. The kanamycin-resistant transformants were identified by PCR (using

117   P7+P8 for the presence of Kan cassette, and P9+P10 for *qseBC* deletion). The target vector pLQ4

118   was built as follows: the fragment was ligated into a linearized vector PSF116, which was digested

119   by Kpn Ι and BamHI using a BM seamless cloning kit (Biomed, Beijing, China). The pLQ5 was

120   introduced into Δ*qseBC* by natural transformation. The complementary strain C-Δ*qseBC* was

121   selected on TSA supplemented with 20 μg/mL gentamicin. The gentamicin-resistant transformants

122   were identified by PCR. The flow chart for construction of the Δ*qseBC* mutant is shown in the

123   attachment (Fig.S1).

124   To rule out the possible polar effects resulting from the deletion of *qseB* and *qseC* genes, relative

125   quantification of 2 ($-\Delta\Delta$C(T)) method was adopted to analyze the transcriptional levels of the

126   flanking genes by quantitative real-time PCR (qRT-PCR) using primer sets P19/P20 for

127   A4U84_RS03675 (hypothetical protein) and P21/22 for *groES* (co-chaperone), respectively. The

128   stably transcriptional 16S RNA of *G. parasuis* was used as an internal reference gene. qRT-PCR

129   was performed by using an iTaqTM universal SYBR Green Supermix (Bio-Rad) in a Lightcycler

130   96 (Roche, Switzerland) system.

131   **Table 2** Primers used in this study.

132   **2.4 Preparation of 3D4/21 cell culture and adhesion and invasion assays**

133   The study was performed as described in previous papers with some modifications (Ji et al.,

134   2017; Xu et al., 2015; Zhou et al., 2016). The colony count method was used to study the adhesion

135   and invasion ability of the Δ*qseBC* mutant strain to host cells. Porcine alveolar macrophages

136 (PAM) 3D4/21 were purchased from Shanghai Zeye Biotechnology Co., Ltd. The 3D4/21 cells

137 were cultured in Dulbecco's modified Eagle's medium (DMEM) supplemented with 10%

138 (v/v) fetal bovine serum (FBS), 100 U/mL of penicillin G (Invitrogen), 100 mg/mL of

139 streptomycin (Invitrogen) and MEM non-essential amino acids (Invitrogen). Cells were cultured

140 at 37°C in a humidified incubator with 5% CO_2 for 12 h before use. Then, cells at more than 80%

141 confluence in 6-well plates were used for subsequent assays.

142 For the adhesion assay, the wild-type SC1401, derivatives of Δ*qseBC* and C-Δ*qseBC* were

143 grown to logarithmic growth. These bacteria were washed in sterile PBS by centrifugation,

144 resuspended in DMEM and adjusted by dilution to a multiplicity of infection (MOI) of 100:1

145 (1×10^7 bacteria vs. 1×10^5 host cells). Plates were incubated at 37°C in 5% CO_2. The cells were

146 incubated for 2h for bacterial adhesion, and then vigorously washed three times with PBS to

147 remove nonspecifically attached bacteria. Then the cells were incubated for 10 min at 37°C with

148 100 μL 0.25% trypsin/0.02% EDTA. After incubation, 900 μL TSB was added, the cells were

149 diluted with 10-fold serial for 4 times and 100 μL cultures were spread on TSA++ plates. The

150 visible colonies were counted manually to calculate the colony forming units (CFU).

151 For the invasion assay, complete growth medium (including 150 μg/mL of gentamicin) was

152 added to each well, and the plates were incubated for additional 2h to kill extracellular *G. parasuis*

153 and washed three times with PBS. The above cells were lysed with 1% Triton X-100 to determine

154 the intracellular bacteria by serial dilutions. The visible colonies were counted manually to

155 calculate the CFU. The assay was performed in triplicates.

156 **2.5 Indirect immunofluorescent assay of adherent bacteria on MLE-12 cells**

157 Mouse lung epithelial cells MLE-12 were purchased from the Beijing Institute of BeNa

158 Biotechnology (ATCC-sourced strain, the 4th passage). In the indirect immunofluorescent (IIF)

159 assay, MLE-12 cells were grown on coverslips in a six-well plate to reach a cell concentration of

160 90% confluence. The bacteria and cells were co-incubated following the adhesion assay. In this

161 study, the *G. parasuis* HpGbpA polyclonal antibody (1:500 dil.) prepared and stored in our

162 laboratory was used as the primary antibody, and the commercial CY3-labeled goat anti-mouse

163 IgG (Servicebio) was used as the secondary antibody to detect the distribution of bacteria. Cy3-

164 labeled fluorescent secondary antibodies (EX WL: 510–560 nm, EM WL: 590 nm) were detected

165 by a fluorescence microscope Nikon Eclipse ci&NIKON DS-U3, and the fluorescence intensity

166 was analyzed by CaseViewer software. Fluorescence signal intensity was analyzed using

167 ImageProPlus software and expressed as integrated optical density (IOD). The relative IOD value

168 (IOD_R) is the ratio of the fluorescence intensity of CY3 (IOD_C) to the fluorescence intensity of

169 DAPI (IOD_D).

170 **2.6 Animal infection studies**

171 Animal infection studies were performed as described previously (Dai et al., 2019a; Dai et al.;

172 Ding et al., 2016; Zhang et al., 2016). All efforts were made to provide for maximum comfort and

173 minimal suffering of the animals. The study was conducted in accordance with ethic guidelines of

174 the recommendations in the China Regulations for the Administration of Affairs Concerning

175 Experimental Animals (1988) and the study was approved by the Institutional Animal Care and

176 Use Committee of Southwest Medical University (20211017-001), Sichuan, China.

177 Thirty-two mice were allocated randomly to 4 groups of 8. Three groups were intraperitoneally

178 injected with the *G. parasuis* SC1401, Δ*qseBC* or C-Δ*qseBC* strain at a dose of 1.3×10^8 CFU per

179 mouse. The remaining group was allocated to the PBS control group and injected intraperitoneally

180 with 0.5 mL PBS. Dying animals that exhibited lethargy, hunched backs, rough coats, swollen

181 abdomens, or inability to eat or drink were euthanized and considered dead.

182 Random block grouping method: mice were allocated randomly to SC1401, Δ*qseBC*, C-

183 Δ*qseBC* and mock groups, with each group containing 8 randomized mice. The random number

184 table was then used to randomly assign the animals to the treatment group and the control group

185 for experimental observation. In order to reduce the differences in experiments for non-research

186 purposes, when the animals were injected intraperitoneally, groups were randomly selected, and a

187 new set of syringes and needles was used for each individual animal. The animal cages were placed

188 on the same level in the cage rack. In this blinded experiment, animal management personnel were

189 not informed about the animal groupings, and the observations were done without information on

190   the grouping of animals, so as to reduce the artificial selection bias in the observation of the results.

191   All mice were intraperitoneally injected with bacteria at a dose of 1.3×10^8 CFU/animal (0.5 mL)

192   or with 0.5 mL PBS. Clinical symptoms were carefully monitored for 7 days. Euthanasia was

193   carried out on the animals with sleepiness, hunchback posture, rough hair, abdominal distension,

194   or inability to eat or drink. The method of euthanasia was intraperitoneal injection of sodium

195   pentobarbital (150 mg/kg). After 72 hours of challenge, 3 animals in each group were euthanized

196   humanely. The spleens and lungs were autopsied and treated with formalin/paraformaldehyde-

197   fixed, paraffin-embedded (FFPE), and used for hematoxylin eosin (H&E) analysis to determine

198   the pathological damage before and after immunization. The surviving mice were humanely

199   euthanized (7 dpi).

200   **2.7 Histological Examination (H&E) and immunofluorescence assay**

201   Mice were euthanized using sodium pentobarbitone (150 mg/kg). Lung and spleen tissues were

202   harvested from mice in different groups (SC1401, $\Delta qseBC$,C-$\Delta qseBC$ and PBS) after 4 dpi and

203   fixed with 4% paraformaldehyde for histopathological and immunofluorescence (IF) assay. The

204   paraffin sections were deparaffinized to water, and the sections were stained with hematoxylin and

205   eosin (H&E) in turn, dehydrated, sealed with neutral gum and examined under a microscope (Dai

206   et al.).

207   Myeloperoxidase (MPO) levels were measured through the IF assay to quantitatively evaluate

208   the levels of inflammation in the lungs of mice infected with SC1401,$\Delta qseBC$ and $\Delta qseC$. The

209   experimental procedure is described in Dai et al (Dai et al., 2019a). Mouse tissue and partial

210   preparations were similar to the preparation of H&E materials. The fluorescent secondary antibody

211   labeled with CY3 (EX WL: 510–560 nm, EM WL: 590 nm) was detected by a fluorescent

212   microscope Nikon Eclipse ci&NIKON DS-U3, and the fluorescence intensity was analyzed by

213   CaseViewer software. Fluorescence signal intensity was analyzed using ImageProPlus software

214   and expressed as integrated optical density (IOD). The relative IOD value (IOD_R) is the ratio of

215   the fluorescence intensity of CY3 (IOD_C) to the fluorescence intensity of DAPI (IOD_D).

216   **2.8 Determination of the level of apoptosis in lung tissue (TUNEL staining)**

217   In order to study cell apoptosis in situ in mice, the lungs of mice in the SC1401, $\Delta qseBC$ and

218    $\Delta qseC$ challenge groups were collected, and then the TUNEL (TdT-mediated dUTP nick end

219   labeling) kit was used to detect the level of apoptosis (Dai et al., 2019a). Fluorescence microscope

220   Nikon Eclipse ci&NIKON DS-U3 was used to detect FITC-labeled fluorescent secondary antibody

221   (EX WL: 465-495 nm, EM WL: 515-555 nm)), and the fluorescence intensity was analyzed by

222   CaseViewer software. Fluorescence signal intensity was analyzed using ImageProPlus software

223   and expressed as integrated optical density (IOD). The relative IOD value (IOD_R) is the ratio of

224   the fluorescence intensity of FITC (IOD_F) to the fluorescence intensity of DAPI (IOD_D).

225   **2.9 Statistical analyses**

226   Statistical analyses were performed using Graph-Pad Prism 5.0 software (GraphPad Software,

227   San Diego, CA, USA). A one-way or two-way ANOVA analysis was used to compare the

228   differences among more than two groups. P values < 0.05 were considered statistically significant.

229   **3. Results**

230   **3.1 The *qseB* and *qseC* genes are conserved among 15 standard strains of *G. parasuis***

231   The standard strains of *G. parasuis* 1-15 were used as the templates to amplify the *qseB* and

232   *qseC* genes by PCR, and the target bands were obtained (*qseB* is 672 bp; *qseC* is 1398 bp). It was

233   shown that the 15 standard strains of *G. parasuis* serotype all have *qseB* and *qseC* genes (Figure1

234   A/B).

235   **Figure 1. Amplification of *qseB* gene (A) and *qseC* gene (B) from serotypes 1-15 of *G. parasuis* standard**

236   **strains.** M: DL5000 DNA marker;1-15: Serotypes 1-15 of *G. parasuis* standard strains.

237   **3.2 Validation of the *qseB/C* genes deletion and complementation**

238   The recombinant plasmid pLQ4 was identified by restriction enzyme digestion (Figure 2A). The

239   recombinant plasmid pLQ4 was digested into a vector fragment (5600 bp) and an insert fragment

240   (2840 bp). The in-frame nonpolar $\Delta qseBC$ mutant was constructed by natural transformation and

241   confirmed by PCR (Figure 2B). The identities of SC1401, $\Delta qseBC$ and C-$\Delta qseBC$ were confirmed

242   in all strains by amplifying the 822-bp fragment encoding 16S rRNA using primers P11/P12. A

243   2061-bp fragment of the *qseBC* gene using primers P9/P10 was amplified from the wild type and

244   complement, but not the mutant. The kan fragment (935 bp) was amplified using primers P7/P8

245   from the mutant and complement, but not from the wild-type strain SC1401, indicating that the

246   gene mutant and its complemented strain were successfully constructed.

247   The transcription of the *qseB* and *qseC* flanking genes were further examined by RT-qPCR to

248   assess the possible polar effects caused by deletion of the *qseB* and *qseC* genes. As shown in

249   SC1401 and ΔqseBC, both the upstream gene A4U84_RS03675 and downstream gene *groES* were

250   not significantly affected (Figure 2C), indicating no polar effect.

251   **Figure 2. Construction and verification of the *qseBC* mutant and the complemented strain (*qseB* and *qseC***

252   **have a 14-bp overlap).** (A) Identification of the recombinant plasmid pLQ4 (lane 1: BamHI; lane 2: EcoR Ⅰ

253   and BamH Ⅰ) by restriction enzyme digestion. (B) PCR identification of strains SC1401, ΔqseBC and C-

254   ΔqseBC. Lane 1, 4, 7: primers HPS-F/HPS-R amplify HPS 16S rRNA gene; lane 2, 5, 8: primers *qseBC*-

255   F/*qseBC*--R amplify *qseB* and *qseC* genes; lane 3, 6, 9: primers Kan-F/Kan-R amplify the kan gene. (C) RT-

256   qPCR verification of polar effect. Transcription levels of the neighbouring genes in the ΔqseBC mutant

257   were determined by RT-qPCR using 16S rRNA as an internal control.

258   **3.3 The Δ*qseBC* mutant decreased adherence and invasion abilities**

259   In order to further study the effect of *G. parasuis* two-component system QseBC on the

260   interaction between bacteria and host cells, the PAM cells were co-incubated with SC1401,

261   ΔqseBC and ΔqseC to compare their adhesion and invasion abilities. As shown in Figure 3A/B,

262   using bacteria in the same growth state (taking OD_{600}nm as a reference) and the same batch of

263   plated cells, when MOI=100, the average number of cells adhered to PAM cells by SC1401,

264   ΔqseBC and ΔqseC were 311.67×10^5 CFU/well, 178.67×10^5 CFU/well and 223.33×10^5 CFU/well,

265   respectively. As compared to the parent strain, both mutant strains showed a significant decrease.

266   In addition to the decreased number of adhesions, deletion of the *qseB/C* genes also significant

267   impaired the ability of the bacteria to invade the PAM cells ($p<0.05$). The adhesion and invasion

268   levels were recovered in the complemented strain C-ΔqseBC.

269   In addition, the decreased adhesion of ΔqseBC and ΔqseC to mouse-derived MLE-12 cells was

270   observed using the IIF assay. The HpGbpA polyclonal antibody (1:500 dil.) prepared and stored

271   in our laboratory was used as the primary antibody, and the commercial Cy3-labeled goat anti-

272   mouse IgG (Servicebio) was used as the secondary antibody to climb the slides of MLE-12 cells.

273   Indirect immunofluorescence assay was performed. The DAPI (blue) column represents the

274   nuclear staining results; the CY3 column (red) represents the bacterial staining results; the third

275   column is the combined graph of the two (observing the results of bacterial adherent cells).

276   Fluorescence signal intensities are displayed as integrated optical density (IOD) values and

277   analyzed by ImageProPlus software. The relative value of IOD_R was calculated by the ratio of

278   Cy3-fluorescence intensity (IOD_C) and IOD of DAPI (IOD_D). As shown in Figure 3C/D, the

279   relative fluorescence intensity (RFI) of the deletion strain was significantly lower than that of the

280   parent strain, and the red fluorescence was localized on the cell surface, which was consistent with

281   the location of bacteria adhering to the cell surface. The results of this part further confirmed that

282   the QseBC two-component system was involved in the regulation of bacterial adhesion to cells.

283   In summary, our results indicated that $\Delta qseBC$ resulted in a significant decrease in the adhesion

284   and invasion abilities of the bacteria to the PAM and MLE-12 cells used in the experiment,

285   suggesting that QseBC affects the ability of the bacteria to interact with PAM and MLE-12 cells.

286   **Figure 3. Adhesion and invasion abilities of *G. parasuis* to PAM and MLE-12 cells.** (A) Adhesion to PAM

287   cells. (B) Invasion to PAM cells. (C) Indirect immunofluorescent analysis (IIF) of adherent $\Delta qseBC$ and $\Delta qseC$

288   mutants to MLE-12 cells. IIF assays were conducted to detect the distribution of bacteria by mouse-derived

289   HpGbpA polyclonal antibody (1:500 dil.) and Cy3-conjugated goat-anti-mouse IgG (Servicebio). (D) Statistical

290   analysis of IOD of MLE-12 cells. Relative values of IOD_R were calculated by the ratio of the IOD of CY3-

291   fluorescence intensity (IOD_C) and DAPI (IOD_D). The experiments were performed in triplicates. Error bars

292   represent the standard errors from three independent experiments.

293   **3.4 Decreased virulence of the $\Delta qseBC$ mutant in mice**

294   The SC1401 and the $\Delta qseC$ or $\Delta qseBC$ strain were compared in a murine model of infection.

295   After intraperitoneal injection with SC1401, the survival rate was 12.5% (1 mouse), whereas the

296   survival rate was 50% (4 mice) in both the $\Delta qseBC$ and $\Delta qseC$ groups. No anomalies were

297   observed in the PBS control group throughout the entire virulence assays. In short, 87.5% of mice

298 inoculated with SC1401 died as compared to only 50% of mice inoculated with Δ*qseBC* and

299 Δ*qseC*, respectively (Figure 4A), demonstrating that QseBC contributes to the virulence of *G.*

300 *parasuis*.

301 Lung and spleen tissues of hosts were harvested for histological pathological observation using

302 H&E staining. As shown in Figure 4B/C, pathological lesions were present in all treated groups.

303 The mice in wild-type and complemented groups showed severe congestion of alveolar wall

304 capillaries. However, mice in Δ*qseC* and Δ*qseBC* groups demonstrated less severe pathological

305 changes.

306 **Figure 4. Survival curves of mice challenged with *G. parasuis* and histopathologic analysis of lungs and**

307 **spleens (200×).** (A) Survival curves of mice infected intraperitoneally with SC1401, Δ*qseBC*, Δ*qseC* or C-

308 Δ*qseBC* strains. The survival percentage of mice infected with Δ*qseBC* or Δ*qseC* was significantly higher

309 than that of the wild-type strain using the log-rank test (P<0.05). (B) Lung tissues of mice challenged with *G.*

310 *parasuis*. **Mock group** (Mock): There was no obvious abnormality in the morphology and structure of the

311 airway; a small amount of alveolar wall thickening (black arrow) with scattered inflammatory cell infiltration

312 (yellow arrow) can be seen. **Wild-type group** (SC1401): There was no obvious abnormality in the morphology

313 and structure of the airway; extensive alveolar wall capillary hyperemia (black arrow) and narrow alveolar cavity

314 can be seen; vascular congestion was more common (blue arrow); no obvious inflammatory cell infiltration seen.

315 ***qseC* mutant group** (Δ*qseC*): There was no obvious abnormality in the morphology and structure of the airway;

316 a large area of the alveolar wall was slightly thickened (black arrow), accompanied by scattered inflammatory

317 cell infiltration (yellow arrow). ***qseBC* mutant group** (Δ*qseBC*): There was no obvious abnormality in the

318 morphology and structure of the tissue airway; more alveolar walls were slightly thickened (black arrows), and

319 some alveolar cavities were narrowed with scattered inflammatory cell infiltration (yellow arrows); a small

320 number of alveolar sacs were slightly expanded (Blue arrow). ***qseBC* complemented group** (C-Δ*qseBC*): There

321 was no obvious abnormality in the morphology and structure of the airway; more severe congestion of the

322 alveolar wall capillaries (black arrow) was seen; no obvious inflammatory cell infiltration seen. (C) Spleen

323 tissues of mice challenged with *G. parasuis*. **Mock group** (Mock): Abundant white pulp was seen in the tissues,

324 some white pulps were enlarged in volume and some had irregular shapes (black arrows); a few germinal centers

325 (blue arrows) were seen in the white pulp; sinus dilation observed. **Wild-type group** (SC1401): The white pulp

326 of the tissue was severely damaged and the number of lymphocytes was greatly reduced, with only a few

327 remaining present; severe lymphoid necrosis (black arrow), nuclei fragmentation, pyknosis, disappearance, and

328 bleeding of the white pulp (blue arrow) were observed; red; pulp congestion and bleeding seen (green arrow).

329 ***qseC* mutant group** (Δ*qseC*): The tissue white pulp and red pulp cells were plasmacytoid lymphocytes; the

330 white pulp was moderately damaged and the number of lymphocytes was reduced; moderate lymphoid necrosis

331 (black arrow) and nuclei fragmentation can be seen; a large number of red pulp sinus dilatation (blue Arrow) in

332 a honeycomb shape was seen. ***qseBC* mutant group** (Δ*qseBC*): The tissues of the white pulp and red pulp cells

333 were plasmacytoid lymphocytes; the white pulp was slightly injured and the number of lymphocytes was

334 reduced; some lymphoid necrosis (black arrow) and nuclei fragmentation was seen; a large amount of red pulp

335 sinus expansion (blue arrow), in a honeycomb shape was seen. ***qseBC* complemented group** (C-Δ*qseBC*): The

336 white pulp of the tissue was severely damaged and the lymphocytes were significantly reduced, with only a few

337 lymphocytes remaining; severe lymphoid necrosis (black arrow), nuclei fragmentation, pyknosis, and

338 disappearance was seen; red pulp congestion and hemorrhage (blue arrow).

339 **3.5 MPO immunofluorescence analysis**

340 In this experiment, through the IF analysis of the lung pathological tissue of the infected mice,

341 it was found that 4 days after infection (4 dpi), the IOD of the lung tissue of the mice in each

342 treatment group was significantly higher than that of the blank group ($p < 0.05$), suggesting that

343 the activity of MPO was increased. The IOD_R of SC1401 (average IOD_R: 0.625) and

344 complemented groups (average IOD_R: 0.582) were significantly higher than that of the Δ*qseBC*

345 mutant group (average IOD_R: 0.190) and Δ*qseC* mutant group (average IOD_R: 0.371), indicating

346 that Δ*qseBC* and Δ*qseC* mutants caused significantly lower secondary inflammatory active

347 substances in the lungs of mice than the parent strain, and the inflammatory damage to the target

348 tissues may be more minor (Figure 5). The evaluation results of the above pathological sections

349 were further confirmed.

350 **Figure 5. Immunofluorescent (IF) assay for the level of myeloperoxidase (MPO) in lung tissues.** Lung

351 tissues were harvested from mice in different groups after 4 dpi and used for FFPE treatment, pathological slice

352   preparation, and IF assay for MPO. (**A**) IF analysis of lung tissue slides (100×). (**B**) Statistical analysis of IOD

353   of myeloid cells (Biomarker: MPO) in mice lungs. Relative values of IOD_R were calculated by the ratio of the

354   IOD of CY3-fluorescence intensity (IOD_C) and DAPI (IOD_D). The experiments were performed in triplicates.

355   Error bars represent the standard errors from three independent experiments.

356   **3.6 Analysis of tissue apoptosis level in challenged mice**

357   In order to directly observe the pathological damage at the level of cell death, the level of

358   bacterial-induced apoptosis in mouse lungs was quantitatively analyzed by TUNEL staining. As

359   shown in Figure 6, the IOD of the FITC-labeled fluorescent secondary antibody was significantly

360   enhanced in all treatment groups. Taking the IOD_D of DAPI in each group as a reference, the

361   average IOD_R values of mice in the $\Delta qseBC$ and $\Delta qseC$ challenge groups were only 18.88% and

362   16.78% of the parental strain challenge groups, respectively. The mean IOD_R of $\Delta qseBC$ and

363   $\Delta qseC$ were 0.027 and 0.024, respectively, while the IOD_R of the wild-type SC1401 group was

364   0.143. Replenishing strain group can compensate for a certain degree of cell damage ability

365   (average IOD_R=0.098). However, the connection between QseBC and some apoptosis-mediated

366   pathways is uncertain and needs to be further studied in the future.

367   **Figure 6. Apoptosis assay for the level of pathological lesion in lung tissues (TUNEL staining).** Lung tissues

368   were harvested from mice in different groups after 4 dpi and used for FFPE treatment, pathological slice

369   preparation, and IF assay for apoptosis. (**A**) IF analysis (100×). (**B**) Statistical analysis of IOD of myeloid cells

370   (Biomarker: mpo) in mice lungs. Relative values of IOD_R were calculated by the ratio of the IOD of FITC-

371   fluorescence intensity (IOD_F) and DAPI (IOD_D).

372   **4. Discussion**

373   *Glaesserella parasuis* (*G. parasuis*), a common pathogenic bacterium in the upper respiratory

374   tract of pigs (Zhao et al., 2018), is currently one of the main bacterial pathogens harming most of

375   the pig industry in China and even across the world. The currently reported *G. parasuis* virulence

376   factors mainly include: bacterial adhesion factors (outer membrane proteins OmpA/OmpP5 and

377   OmpP2, fimbriae system PilABCD, etc.) (Varela et al., 2014), self-regulation and survival-related

378   factors (binary transduction system ArcAB, QseBC, etc.) (Ding et al., 2016; He et al., 2018; He et

379   al., 2016), bacterial invasion related factors (collagenase PrtC, brain tissue invasion related SphB),

380   bacterial immune evasion factors (GalU and GalE) (Zou et al., 2013), bacterial iron synthesis and

381   uptake proteins (transferrin receptor Tbp) (Gutiérrez-Martín, 2016), and bacterial toxins (Li et al.,

382   2017). Among them, bacterial toxins, mainly including lipopolysaccharide/endotoxin (LPS) (Perry

383   et al., 2013) and cell lethal expansion toxin (CDT family) (Zhang et al., 2012b), are the direct

384   virulence factors of *G. parasuis*, as well as the most important pathogenic factors of *G. parasuis*

385   (Li et al., 2017; Perry et al., 2013). The two-component system QseBC is a ubiquitous signal

386   transmission and gene expression regulation system in bacteria. It participates in the regulation of

387   bacterial growth and reproduction, metabolism, motility, drug resistance and virulence factor

388   expression (Appleby et al., 1996). Inoculation of commercial inactivated vaccines is the main

389   measure to prevent and treat *G. parasuis* infection. However, there are many serotypes of *G.*

390   *parasuis*, and inactivated vaccines will only produce specific antibodies against

391   lipooligosaccharides of the same serotype. Insufficient cross-reactivity makes inactivated vaccines

392   of a single serotype an ineffective means of protection (Dai et al.; Mccaig et al., 2016). Therefore,

393   understanding the molecular mechanism of pathogenicity is essential for the development and

394   targeted therapy of new *G. parasuis* vaccines.

395   The partners of different two-component systems showed significant cross specificity in

396   *Escherichia coli*. Absence of the quorum-sensing *E. coli* (Qse)BC sensor QseC results in a strong

397   cross interaction between its homologous partner QseB and the polymyxin resistance two-

398   component system PmrAB (Kirsten R. Guckesa, 2013). In the absence of homologous sensors,

399   this cross interaction is harmful and seriously weakens the virulence of pathogens. In previous

400   studies, we have constructed the ΔqseB (ΔcheY) and ΔqseC mutant strains, and investigated the

401   functions of QseB and QseC in *G. parasuis*. We found that the ΔqseB mutant strain demonstrated

402   slower growth rate, less biofilms formation and slower agglutination compared with the wild-type

403   strain. However, there were no observed apparent differences of serum-resistance between the wild-

404   type and gene-mutant strain. Moreover, the ΔqseC exhibited a decreased resistance to osmotic

405   pressure, oxidative stress and heat shock. We also found that the ΔqseC had weakened the ability

406   to take up iron and showed defective biofilm formation, and that QseC participated in sensing the

407   epinephrine in environment to regulate the density of *G. parasuis*. However, the entire two-

408   component system QseBC knockout in *G. parasuis* had not been reported. These results

409   encouraged us to study the basic molecular functions of this important signal transduction system

410   in *G. parasuis*. It is still unclear whether the decreased virulence of Δ*qseC* mutant strain is related

411   to the activation of QseB by PmrB, thus requiring further study. It is also not clear whether there

412   is strong crosstalk from other two-component systems in Δ*qseB* and Δ*qseC* mutant strains.

413   Therefore, we knocked out *qseB* and *qseC* double genes to elucidate the role of QseBC in the

414   pathogenicity of *G. parasuis* and provide the basis for further study on the pathogenic mechanism

415   of *G. parasuis*.

416   *Glaesserella parasuis* can invade porcine brain microvascular epithelial cells (PBMEC), which

417   are the main cells in the blood-brain barrier (BBB), indicating that *G. parasuis* can cross the BBB

418   to reach the central nervous system. Previous studies have found that *G. parasuis* has the ability to

419   adhere and invade a variety of cells, such as porcine umbilical artery endothelial cells (PUVEC),

420   porcine kidney epithelial cells (PK-15), alveolar macrophages (PAM) cells, etc. (Bouchet et al.,

421   2008; Zhang et al., 2012a; Zhou et al., 2012). However, more in-depth research is needed to

422   elucidate the molecular mechanism by which *G. parasuis* breaks through the mucosal barrier. In

423   this study, we found that deletion of the *qseBC* gene resulted in a significant decrease in the ability

424   of *G. parasuis* to adhere to host cells. It was confirmed that similar to *Actinobacillus*

425   *pleuropneumoniae*, the two-component system QseBC in *G. parasuis* may regulate bacterial

426   adhesion by regulating the expression of downstream virulence genes (Liu et al., 2015). Based on

427   the above results, we hypothesize that the loss of *qseBC* gene expression leads to a decrease in the

428   ability of the pathogenic bacteria to adhere and invade host cells, which may be part of the reason

429   for the weakened virulence of *G. parasuis*.

430   Animal infection studies in this study further assess the importance of the QseBC two-

431   component system. We combined our findings in this study with our previous study that showed

432   that the QseBC two-component system functions as a global virulence regulator (Weigel and

433 Demuth, 2016). We verified that deletion of *qseBC* genes in *G. parasuis* can lead to attenuated

434 virulence in the BALB/c mouse model. Mice infected with the Δ*qseBC* mutant had a 37.5%

435 reduction in mortality as compared to mice infected with SC1401 (Figure 4). This is similar to the

436 results of *qseB* or *qseC* gene deletion in *Haemophilus influenzae* (Wang et al., 2011). In order to

437 understand how the lack of QseBC affects the pathogenicity of *G. parasuis*, we collected mouse

438 lungs and spleens for pathological sectioning, observed and compared the pathological changes,

439 and found that the Δ*qseBC* mutant caused low fatal infection rate and relatively mild pathological

440 damage. The alveolar wall was slightly thickened with scattered inflammatory cell infiltration in

441 the Δ*qseC* group. In the Δ*qseBC* group, more alveolar walls were found to be slightly thickened,

442 and some alveolar cavities were narrowed with scattered inflammatory cell infiltration, with a

443 small number of alveolar sacs observed to be slightly expanded (Figure 4B). In the spleen tissues

444 of mice in wild-type groups, the white pulp was severely damaged and displayed dilatation, and

445 the number of lymphocytes was greatly reduced, with only a few lymphocytes remaining present.

446 Moreover, severe lymphoid necrosis, nuclei fragmentation, pyknosis, disappearance, and bleeding

447 of the white pulp in the tissues were observed. However, in the Δ*qseC* group, the tissues of the

448 white pulp and red pulp cells were plasma cell-like lymphocytes; white pulp was moderately

449 injured, with reduced number of lymphocytes, and more lymphoid necrosis and nuclear

450 fragmentation were seen; a large number of red pulp sinuses were expanded in a honeycomb

451 pattern. In the Δ*qseBC* group, the tissues of the white pulp and red pulp cells were plasmacytoid

452 lymphocytes. Moreover, we observed reduced number of lymphocytes, and slight lymphoid

453 necrosis and nuclei fragmentation in the tissues (Figure 4C). No significant bleeding and dilation

454 of the spinal sinuses were observed in the mock group. This data showed that while the Δ*qseC* and

455 Δ*qseBC* mutants could still cause certain degree of pathological lesion, the symptoms and

456 pathological changes were less pronounced in mutant groups than wild-type and complemented

457 groups, indicating that the deletion of *qseB* and *qseC* genes led to a significant attenuation of the

458 degree of pathological damage caused by *G. parasuis* in the mouse model.

459 Indirect immunofluorescence assays were performed on mouse lungs to compare

460   myeloperoxidase (MPO) levels to assess the development of inflammation. IF analysis showed

461   that the ΔqseBC mutant produced lower levels of oxidative damage and less severe levels of

462   inflammation and apoptosis. In order to directly observe the pathological damage at the level of

463   cell death, the level of bacterial-induced apoptosis in mouse lungs was quantitatively analyzed by

464   TUNEL staining. We confirmed that the rate of apoptosis induced by the ΔqseBC and ΔqseC

465   mutant strains was significantly reduced as compared to the wild strain. In conclusion, our results

466   show that ΔqseBC has weak pathogenicity in mouse models, and its abilities to induce

467   inflammation and apoptosis are significantly lower than that of parental and apoplectic strains for

468   mice treated with the same dose of bacteria. After undergoing the challenge, mice in the mutant

469   strain group had weaker pathological manifestations and lower mortality. This indicates that the

470   QseBC two-component system can significantly regulate the virulence of HPS to the host.

471   Subsequent research can use transcriptomes, proteomes, combined with gene

472   regulation/interaction network, and other means to comprehensively study the regulatory

473   mechanism behind it.

474   **5. Conclusions**

475   In conclusion, our results indicate that QseBC is essential for the bacterial virulence of *G.

476   parasuis* in the mouse model. A key uncertainty factor is that the mouse model cannot reflect the

477   exact infection process of *G. parasuis* in its natural host. The pig should be used as a model to

478   further evaluate the virulence of these strains. Our research can lay the foundation for the follow-

479   up study of the virulence of QseBC in the pig model and contribute to exploring the pathogenic

480   mechanism of *G. parasuis* and the development of *G. parasuis* subunit vaccine.

481   **ACKNOWLEDGEMENTS**

482   We thanked Prof. Liao and Prof. Fan from the College of Veterinary Medicine, South China

483   Agricultural University, Guang zhou, China for their kindly providing the integrative plasmid

484   pSF116.

485   **ADDITIONAL INFORMATION AND DECLARATIONS**

486   **Funding**

487 This work was funded by the Science and Technology Strategic Cooperation Programs of

488 Luzhou Municipal People's Government and Southwest Medical University (2019LZXNYDJ20)

489 and University Sponsered Research Program of Southwest Medical University (2020ZRQNA010).

490 The funding body supported preparation of test materials, and had no role in the design of the study

491 and collection, analysis, and interpretation of data and in writing the manuscript.

492 **Grant Disclosures**

493 The following grant information was disclosed by the authors: The Science and Technology

494 Strategic Cooperation Programs of Luzhou Municipal People's Government and Southwest

495 Medical University: 2019LZXNYDJ20; University Sponsered Research Program of Southwest

496 Medical University: 2020ZRQNA010.

497 **Competing Interests**

498 The authors declare there are no competing interests.

499 **Author contributions**

500 • HLQ conceived and designed the experiments and performed the experiments.

501 • YXF and DK analyzed the data and wrote the paper.

502 • Manli He and Congwei Gu prepared figures and/or tables.

503 • Wudian Xiao and Mingde Zhao reviewed drafts of the paper.

504 **Data Availability**

505 The following information was supplied regarding data availability: The raw data has been

506 provided as a Supplemental File.

507

508

509

510

511

512

513

514

515

516   **References**

517   **Appleby, J.L., Parkinson, J.S., Bourret, R.B., 1996.** Signal transduction via the multi-step phosphorelay: not

518   necessarily a road less traveled. *Cell* **86:**845-848 DOI 10.1016/S0092-8674(00)80158-0.

519   **Bearson, B.L., Bearson, S.M., 2008.** The role of the QseC quorum-sensing sensor kinase in colonization and

520   norepinephrine-enhanced motility of *Salmonella* enterica serovar Typhimurium. *Microb Pathog*

521   **44:**271-278 DOI 10.1016/j.micpath.2007.10.001.

522   **Bouchet, B., Vanier, G., Jacques, M., Gottschalk, M., 2008.** Interactions of *Haemophilus parasuis* and its

523   LOS with porcine brain microvascular endothelial cells. *Veterinary Research* **39:**42 DOI

524   10.1051/vetres:2008019.

525   **Dai, Xiaoyu, Zhen, Yang, Yung-Fu, Chang, Sanjie, Cao, Qin, Zhao, 2019a.** Polyamine Transport Protein

526   PotD Protects Mice against *Haemophilus parasuis* and Elevates the Secretion of Pro-Inflammatory

527   Cytokines of Macrophage via JNK-MAPK and NF-κB Signal Pathways through TLR4. *Vaccines*

528   7(4):216 DOI 10.3390/vaccines7040216.

529   **Dai, K., Yang, Z., Chang, Y.F., He, L., Wen, Y., 2019b.** Construction of targeted and integrative promoter-

530   reporter plasmids pDK-K and pDK-G to measure gene expression activity in *Haemophilus parasuis*.

531   *Microbial Pathogenesis* **134:**103565 DOI 10.1016/j.micpath.2019.103565

532   **Dai, K., Yang, Z., Ma, X., Chang, Y.F., Cao, S., Zhao, Q., Huang, X., Wu, R., Huang, Y., Xia, J.,2021.**

533   Deletion of Polyamine Transport Protein PotD Exacerbates Virulence in Glaesserella (Haemophilus)

534   parasuis in the Form of Non-biofilm-generated Bacteria in a Murine Acute Infection Model. *Vaccines*

535   **12(1):**520–546 DOI 10.1080/21505594.2021.1878673.

536   **Ding, L., Wen, X., He, L., Yan, X., Wen, Y., Cao, S., Huang, X., Wu, R., Wen, Y., 2016.** The *arcA* gene

537   contributes to the serum resistance and virulence of *Haemophilus parasuis* serovar 13 clinical strain

538   EP3. *Vet Microbiol* 196:67-71 DOI 10.1016/j.vetmic.2016.10.011.

539   **Gutiérrez-Martín, C., 2016.** A vaccine based on a mutant transferrin binding protein B of *Haemophilus*

540   *parasuis* induces a strong T-helper 2 response and bacterial clearance after experimental infection.

541     *Veterinary Immunology and Immunopathology* **179:**18-25 DOI 10.1016/j.vetimm.2016.07.011.

542   **He, L., Dai, K., Wen, X., Ding, L., Cao, S., Huang, X., Wu, R., Zhao, Q., Huang, Y., Yan, Q., Ma, X., Han,**

543     **X., Wen, Y., 2018.** QseC Mediates Osmotic Stress Resistance and Biofilm Formation in *Haemophilus*

544     *parasuis*. *Front Microbiol* **9:**212 DOI 10.3389/fmicb.2018.00212.

545   **He, L., Wen, X., Yan, X., Ding, L., Cao, S., Huang, X., Wu, R., Wen, Y., 2016.** Effect of *cheY* deletion on

546     growth and colonization in a *Haemophilus parasuis* serovar 13 clinical strain EP3. *Gene* **577:**96-100

547     DOI 10.1016/j.gene.2015.11.046.

548   **Huang, J., Wang, X., Cao, Q., Feng, F., Xu, X., Cai, X., 2016.** ClpP participates in stress tolerance and

549     negatively regulates biofilm formation in *Haemophilus parasuis*. *Vet Microbiol* **182:**141-149 DOI

550     10.1016/j.vetmic.2015.11.020.

551   **Hughes, D.T., Clarke, M.B., Yamamoto, K., Rasko, D.A., Sperandio, V., 2009.** The QseC adrenergic

552     signaling cascade in Enterohemorrhagic *E. coli* (EHEC). *PLoS Pathog* **5(8) :**e1000553 DOI

553     10.1371/journal.ppat.1000553.

554   **Ji, Y., Li, W., Zhang, Y., Chen, L., Zhang, Y., Zheng, X., Huang, X., Ni, B., 2017.** QseB mediates biofilm

555     formation and invasion in *Salmonella enterica serovar* Typhi. *Microb Pathog* **104:**6-11 DOI

556     10.1016/j.micpath.2017.01.010.

557   **Juarez-Rodriguez, M.D., Torres-Escobar, A., Demuth, D.R., 2013.** *ygiW* and *qseBC* are co-expressed in

558     *Aggregatibacter actinomycetemcomitans* and regulate biofilm growth. *Microbiology* **159:**989-1001

559     DOI 10.1099/mic.0.066183-0.

560   **Kaplan, J.B., Mulks, M.H., 2005.** Biofilm formation is prevalent among field isolates of *Actinobacillus*

561     *pleuropneumoniae*. *Veterinary Microbiology* **108:**89-94 DOI 10.1016/j.vetmic.2005.02.011.

562   **Kielstein, P., Rappgabrielson, V.J., 1992.** Designation of 15 serovars of *Haemophilus parasuis* on the basis of

563     immunodiffusion using heat-stable antigen extracts. *Journal of Clinical Microbiology* **30:**862-865 DOI

564     10.1016/0168-1656(92)90094-P.

565   **Kirsten R. Guckesa, M.K., Erin J. Breland, Alice P. Gu, Carrie L. Shaffer, Charles R. Martinez III, Scott**

566     **J. Hultgren and Maria Hadjifrangiskou, 2013.** Strong cross-system interactions drive the activation

567     of the QseB response regulator in the absence of its cognate sensor. *PNAS* 110:16592–16597 DOI

568   10.1073/pnas.1315320110.

569   **Kostakioti, M., Hadjifrangiskou, M., Pinkner, J.S., Hultgren, S.J., 2009.** QseC-mediated dephosphorylation

570   of QseB is required for expression of genes associated with virulence in uropathogenic *Escherichia coli*.

571   *Mol Microbiol* **73(6):**1020-1031 DOI 10.1111/j.1365-2958.2009.06826.x.

572   **Li, G., Niu, H., Zhang, Y., Li, Y., Xie, F., Langford, P.R., Liu, S., Wang, C., Chang, Y.F., 2017.** *Haemophilus*

573   *parasuis* cytolethal distending toxin induces cell cycle arrest and p53-dependent apoptosis. *Plos One*

574   **12:**e0177199 DOI 10.1371/journal.pone.0177199.

575   **Liu, J., Hu, L., Xu, Z., Tan, C., Yuan, F., Fu, S., Cheng, H., Chen, H., Bei, W., 2015.** *Actinobacillus*

576   *pleuropneumoniae* two-component system QseB/QseC regulates the transcription of PilM, an important

577   determinant of bacterial adherence and virulence. *Vet Microbiol* **177:**184-192 DOI

578   10.1016/j.vetmic.2015.02.033.

579   **Mah, T., 2012.** Biofilm-specific antibiotic resistance. *Future microbiology* **7(9):**1061-1072 DOI

580   10.2217/FMB.12.76.

581   **Mccaig, W.D., Loving, C.L., Hughes, H.R., Brockmeier, S.L., Alain, C., 2016.** Characterization and Vaccine

582   Potential of Outer Membrane Vesicles Produced by *Haemophilus parasuis*. *Plos One* **11:**e0149132 DOI

583   10.1371/journal.pone.0149132.

584   **Moreira, C.G., Weinshenker, D., Sperandio, V., 2010.** QseC mediates *Salmonella enterica* serovar

585   typhimurium virulence *in vitro* and *in vivo*. *Infect Immun* **78:**914-926 DOI 10.1128/IAI.01038-09.

586   **Oliveira, S., Pijoan, C., 2004.** *Haemophilus parasuis*: new trends on diagnosis, epidemiology and control. *Vet*

587   *Microbiol* **99:**1-12 DOI 10.1016/j.vetmic.2003.12.001.

588   **Patrick, S., Melanie, B., 2013.** Cues and regulatory pathways involved in natural competence and

589   transformation in pathogenic and environmental Gram-negative bacteria. *Fems Microbiology Reviews*,

590   **37:**336-363 DOI 10.1111/j.1574-6976.2012.00353.x.

591   **Perry, M.B., Maclean, L.L., Gottschalk, M., Aragon, V., Vinogradov, E., 2013.** Structure of the capsular

592   polysaccharides and lipopolysaccharides from *Haemophilus parasuis* strains ER-6P (serovar 15) and

593   Nagasaki (serovar 5). *Carbohydrate Research* **378:**91-97 DOI 10.1016/j.carres.2013.04.023.

594   **Sperandio, V., Torres, A.G., Jarvis, B., Nataro, J.P., Kaper, J.B., 2003.** Bacteria-host communication: the

595   language of hormones. *Proc Natl Acad Sci USA* **100:**8951-8956 DOI 10.1073/pnas.1537100100.

596   **Unal, C.M., Singh, B., Fleury, C., Singh, K., Chavez de Paz, L., Svensater, G., Riesbeck, K., 2012.** QseC

597   controls biofilm formation of non-typeable *Haemophilus influenzae* in addition to an AI-2-dependent

598   mechanism. *Int J Med Microbiol* **302:**261-269 DOI 10.1016/j.ijmm.2012.07.013.

599   **Varela, J., Amstalden, M.C., Pereira, R.F., Hollanda, L.D., Ceragioli, H., Baranauskas, V., Lancellotti,**

600   **M., 2014.** *Haemophilus influenzae* porine ompP2 gene transfer mediated by graphene oxide

601   nanoparticles with effects on transformation process and virulence bacterial capacity. *Journal of*

602   *Nanobiotechnology*,**12(1):**1-18 DOI 10.1186/1477-3155-12-14 .

603   **Wang, X., Wang, Q., Yang, M., Xiao, J., Liu, Q., Wu, H., Zhang, Y., 2011.** QseBC controls flagellar motility,

604   fimbrial hemagglutination and intracellular virulence in fish pathogen *Edwardsiella tarda*. *Fish*

605   *Shellfish Immunol* **30:**944-953 DOI 10.1016/j.fsi.2011.01.019.

606   **Weigel, W.A., Demuth, D.R., 2016.** QseBC, a two-component bacterial adrenergic receptor and global

607   regulator of virulence in *Enterobacteriaceae* and *Pasteurellaceae*. *Mol Oral Microbiol* **31:**379-397 DOI

608   10.1111/omi.12138.

609   **Xu, F., Wu, C., Guo, F., Cui, G., Zeng, X., Yang, B., Lin, J., 2015.** Transcriptomic analysis of Campylobacter

610   jejuni NCTC 11168 in response to epinephrine and norepinephrine. *Front Microbiol* 6:452 DOI

611   10.3389/fmicb.2015.00452.

612   **Zhang, B., Feng, S., Xu, C., Zhou, S., He, Y., Zhang, L., Zhang, J., Guo, L., Liao, M., 2012a.** Serum

613   resistance in *Haemophilus parasuis* SC096 strain requires outer membrane protein P2 expression.

614   *FEMS Microbiol Lett* **326:**109-115 DOI 10.1111/j.1574-6968.2011.02433.x.

615   **Zhang, B., He, Y., Xu, C., Xu, L., Feng, S., Liao, M., Ren, T., 2012b.** Cytolethal distending toxin (CDT) of

616   the *Haemophilus parasuis* SC096 strain contributes to serum resistance and adherence to and invasion

617   of PK-15 and PUVEC cells. *Vet Microbiol* **157:**237-242 DOI 10.1016/j.vetmic.2011.12.002.

618   **Zhang, J., Xu, C., Shen, H., Li, J., Guo, L., Cao, G., Feng, S., Liao, M., 2014.** Biofilm formation in

619   *Haemophilus parasuis*: relationship with antibiotic resistance, serotype and genetic typing. *Res Vet Sci*

620   **97:**171-175 DOI 10.1016/j.rvsc.2014.04.014.

621   **Zhang, L., Li, Y., Wen, Y., Lau, G.W., Huang, X., Wu, R., Yan, Q., Huang, Y., Zhao, Q., Ma, X., Wen, X.,**

622   **Cao, S., 2016.** HtrA Is Important for Stress Resistance and Virulence in *Haemophilus parasuis*. *Infect*

623   *Immun* **84:**2209-2219 DOI 10.1128/IAI.00147-16.

624   **Zhao, Y., Qin, W., Jie, L., Lin, X., Fang, B., 2018.** Epidemiology of *Haemophilus parasuis* isolates from pigs

625   in China using serotyping, antimicrobial susceptibility, biofilm formation and ERIC-PCR genotyping.

626   *Peerj* **6:**e5040 DOI 10.7717/peerj.5040.

627   **Zhou, M., Zhang, Q., Zhao, J., Jin, M., 2012.** *Haemophilus parasuis* encodes two functional cytolethal

628   distending toxins: CdtC contains an atypical cholesterol recognition/interaction region. *PLoS One*

629   **7:**e32580 DOI 10.1371/journal.pone.0032580.

630   **Zhou, Q., Feng, S., Zhang, J., Jia, A., Yang, K., Xing, K., Liao, M., Fan, H., 2016.** Two Glycosyltransferase

631   Genes of *Haemophilus parasuis* SC096 Implicated in Lipooligosaccharide Biosynthesis, Serum

632   Resistance,   Adherence,   and   Invasion.   *Front   Cell   Infect   Microbiol*   **6:**100   DOI

633   10.3389/fcimb.2016.00100.

634   **Zou, Y., Feng, S., Xu, C., Zhang, B., Zhou, S., Zhang, L., He, X., Li, J., Yang, Z., Liao, M., 2013.** The role

635   of *galU* and *galE* of *Haemophilus parasuis* SC096 in serum resistance and biofilm formation. *Vet*

636   *Microbiol* **162:** 278-284 DOI 10.1016/j.vetmic.2012.08.006.

637

Figure 1

Amplification of *qseB* gene (A) and *qseC* gene (B) from serotypes 1-15 of *G. parasuis* standard strains.

M: DL5000 DNA marker;1-15: Serotypes 1-15 of *G. parasuis* standard strains.
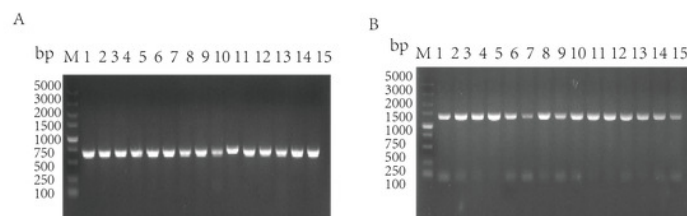
low4

Figure 2

Construction and verification of the *qseBC* mutant and the complemented strain (*qseB* and *qseC* have a 14-bp overlap).

(A) Identification of the recombinant plasmid pLQ4 (lane 1: BamHI; lane 2: EcoR I and BamH I) by restriction enzyme digestion. (B) PCR identification of strains SC1401, Δ*qseBC* and C-Δ*qseBC*. Lane 1, 4, 7: primers HPS-F/HPS-R amplify HPS 16S rRNA gene; lane 2, 5, 8: primers *qseBC*-F/*qseBC*--R amplify *qseB* and *qseC* genes; lane 3, 6, 9: primers Kan-F/Kan-R amplify the kan gene. (C) RT-qPCR verification of polarity effect. Transcription levels of the neighbouring genes in the Δ*qseBC* mutant were determined by RT-qPCR using 16S rRNA as an internal control.
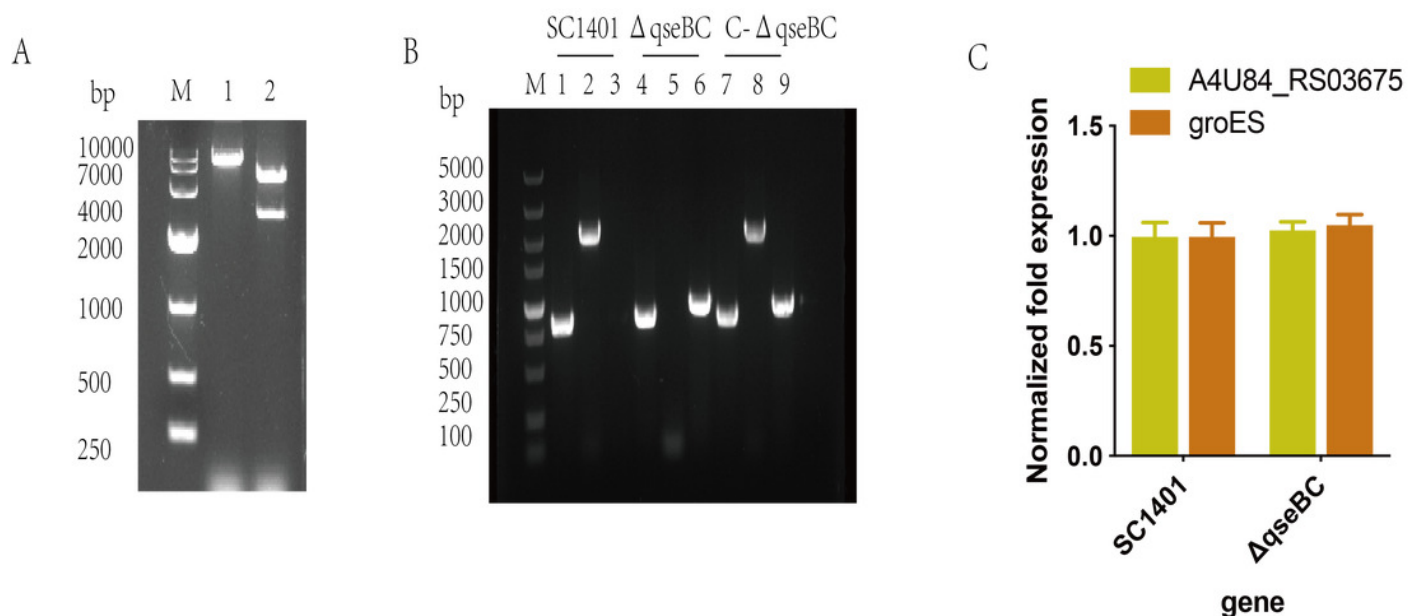
Figure 3

Adhesion and invasion abilities of *G. parasuis* to PAM and MLE-12 cells .

(A) Adhesion to PAM cells. (B) Invasion to PAM cells. (C) Indirect immunofluorescent analysis (IIF) of adherent Δ*qseBC* and Δ*qseC* mutants to MLE-12 cells. IIF assays were conducted to detect the distribution of bacteria by mouse-derived HpGbpA polyclonal antibody (1:500 dil.) and Cy3-conjugated goat-anti-mouse IgG (Servicebio). (D) Statistical analysis of IOD of MLE-12 cells. Relative values of IOD_R were calculated by the ratio of the IOD of CY3-fluorescence intensity (IOD_C) and DAPI (IOD_D). The experiments were performed three times independently in triplicates. Error bars represent the standard errors from three independent experiments.

A

B

C

| | DAPI | CY3 | MERGE |

D
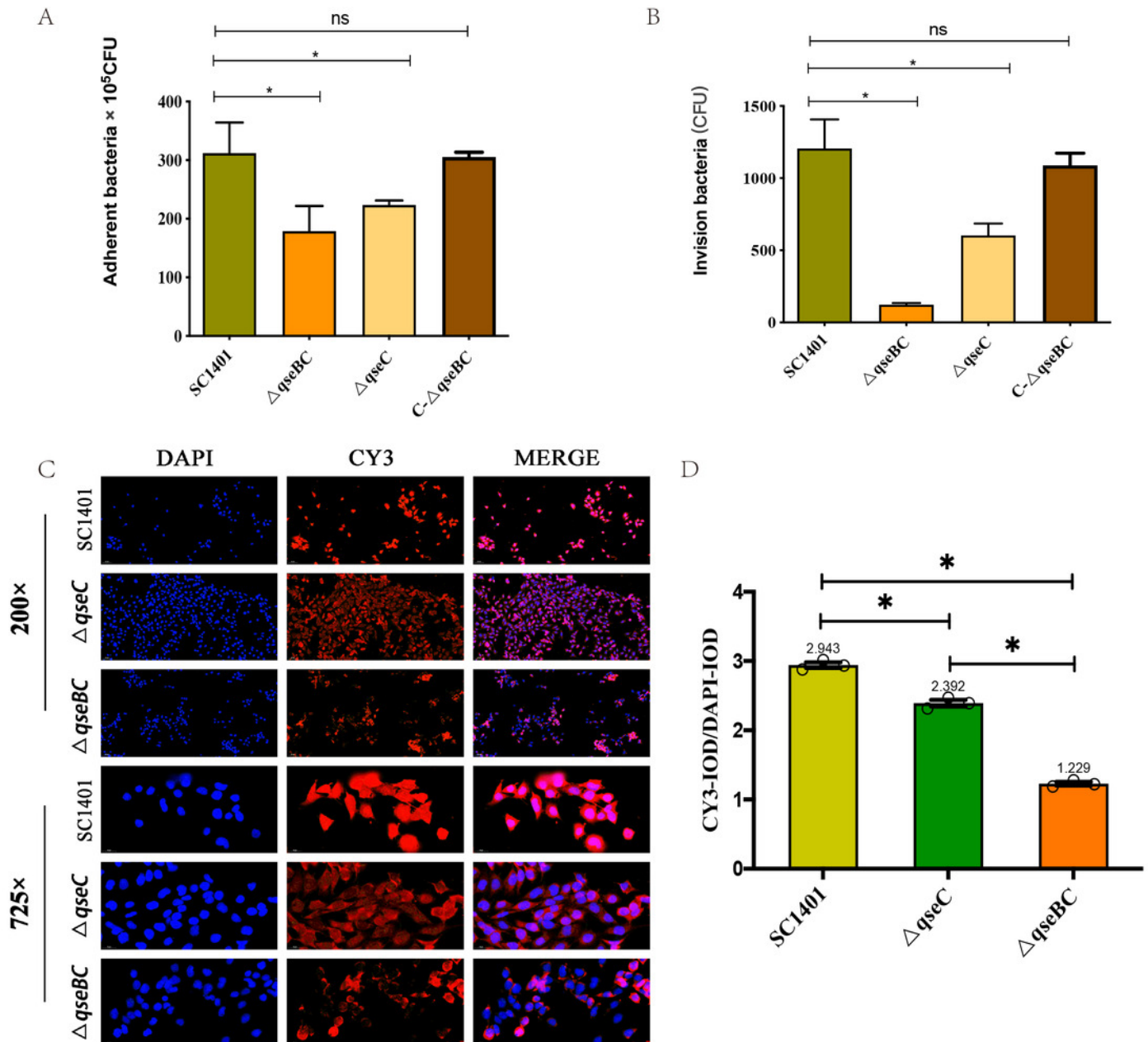
Figure 4

Survival curves of mice challenged with *G. parasuis* and histopathologic analysis of lungs and spleens (200×).

(A) Survival curv es of mice infected intraperitoneally with SC1401, △qseBC, △qseC or C-△qseBC strains. The survival percentage of mice infected with △qseBC or △qseC was significantly higher than that of the wild-type strain using the log-rank test (P<0.05). (B) Lung tissues of mice challenged with *G. parasuis*. **Mock group** (Mock): There was no obvious abnormality in the morphology and structure of the airway; a small amount of alveolar wall thickening (black arrow) with scattered inflammatory cell infiltration (yellow arrow) can be seen. **Wild-type group** (SC1401): There was no obvious abnormality in the morphology and structure of the airway; extensive alveolar wall capillary hyperemia (black arrow) and narrow alveolar cavity can be seen; vascular congestion was more common (blue arrow); no obvious inflammatory cell infiltration seen. *qseC* **mutant group** (ΔqseC): There was no obvious abnormality in the morphology and structure of the airway; a large area of the alveolar wall was slightly thickened (black arrow), accompanied by scattered inflammatory cell infiltration (yellow arrow). *qseBC* **mutant group** (ΔqseBC): There was no obvious abnormality in the morphology and structure of the tissue airway; more alveolar walls were slightly thickened (black arrows), and some alveolar cavities were narrowed with scattered inflammatory cell infiltration (yellow arrows); a small number of alveolar sacs were slightly expanded (Blue arrow). *qseBC* **complemented group** (C-ΔqseBC): There was no obvious abnormality in the morphology and structure of the airway; more severe congestion of the alveolar wall capillaries (black arrow) was seen; no obvious inflammatory cell infiltration seen. (C) Spleen tissues of mice challenged with *G. parasuis*. **Mock group** (Mock): Abundant white pulp was seen in the tissues, some white pulps were enlarged in volume and some had irregular shapes (black arrows); a few germinal centers (blue arrows) were seen in the white pulp;

sinus dilation observed. **Wild-type group** (SC1401): The white pulp of the tissue was severely damaged and the number of lymphocytes was greatly reduced, with only a few remaining present; severe lymphoid necrosis (black arrow), nucle i fragmentation,pyknosis, disappearance, and bleeding of the white pulp (blue arrow) were observed; red; pulp congestion and bleeding seen (green arrow). ***qseC* mutant group** (Δ*qseC*): The tissue white pulp and red pulp cells were plasmacytoid lymphocytes; the white pulp was moderately damaged and the number of lymphocytes was reduced; moderate lymphoid necrosis (black arrow) and nuclei fragmentation can be seen; a large number of red pulp sinus dilatation (blue Arrow) in a honeycomb shape was seen. ***qseBC* mutant group** (Δ*qseBC*): The tissues of the white pulp and red pulp cells were plasmacytoid lymphocytes; the white pulp was slightly injured and the number of lymphocytes was reduced; some lymphoid necrosis (black arrow) and nuclei fragmentation was seen; a large amount of red pulp sinus expansion (blue arrow), in a honeycomb shape was seen. ***qseBC* complemented group** (C-Δ*qseBC*): The white pulp of the tissue was severely damaged and the lymphocytes were significantly reduced, with only a few lymphocytes remaining; severe lymphoid necrosis (black arrow), nuclei fragmentation, pyknosis, and disappearance was seen; red pulp congestion and hemorrhage (blue arrow).
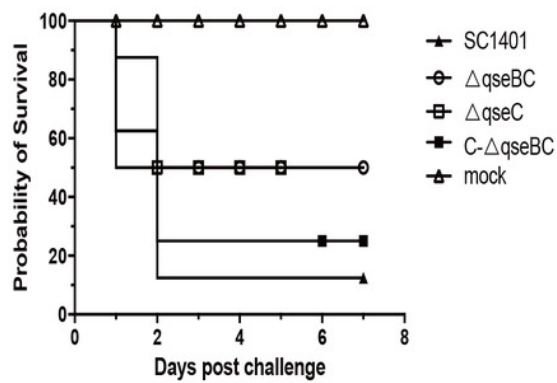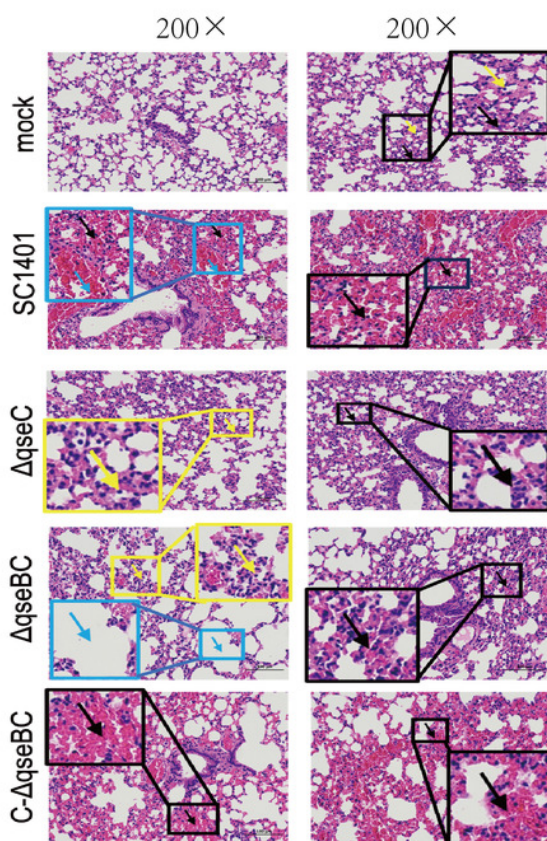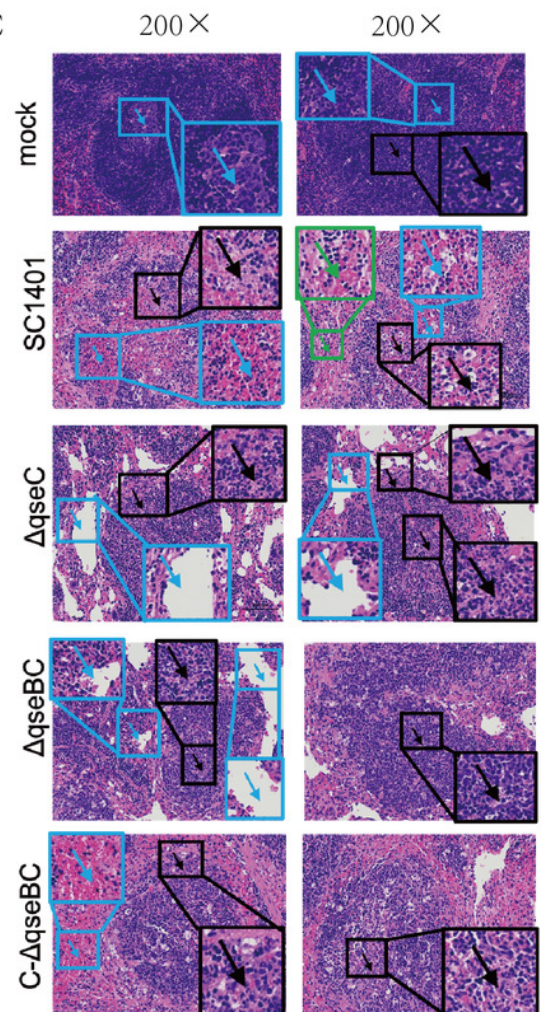
Figure 5

Immunofluorescent (IF) assay for the level of myeloperoxidase (MPO) in l ung tissues.

Lung tissues were harvested from mice in different groups after 4 dpi and used for FFPE treatment, pathological slice preparation, and IF assay for MPO. (**A**) IF analysis of lung tissue slides (100×). (**B**) Statistical analysis of IOD of myeloid cells (Biomarker: MPO) in mice lungs. Relative values of IOD_R were calculated by the ratio of the IOD of CY3-fluorescence intensity (IOD_C) and DAPI (IOD_D). T he experiments were performed three times independently in triplicates. Error bars represent the standard errors from three independent experiments.

A
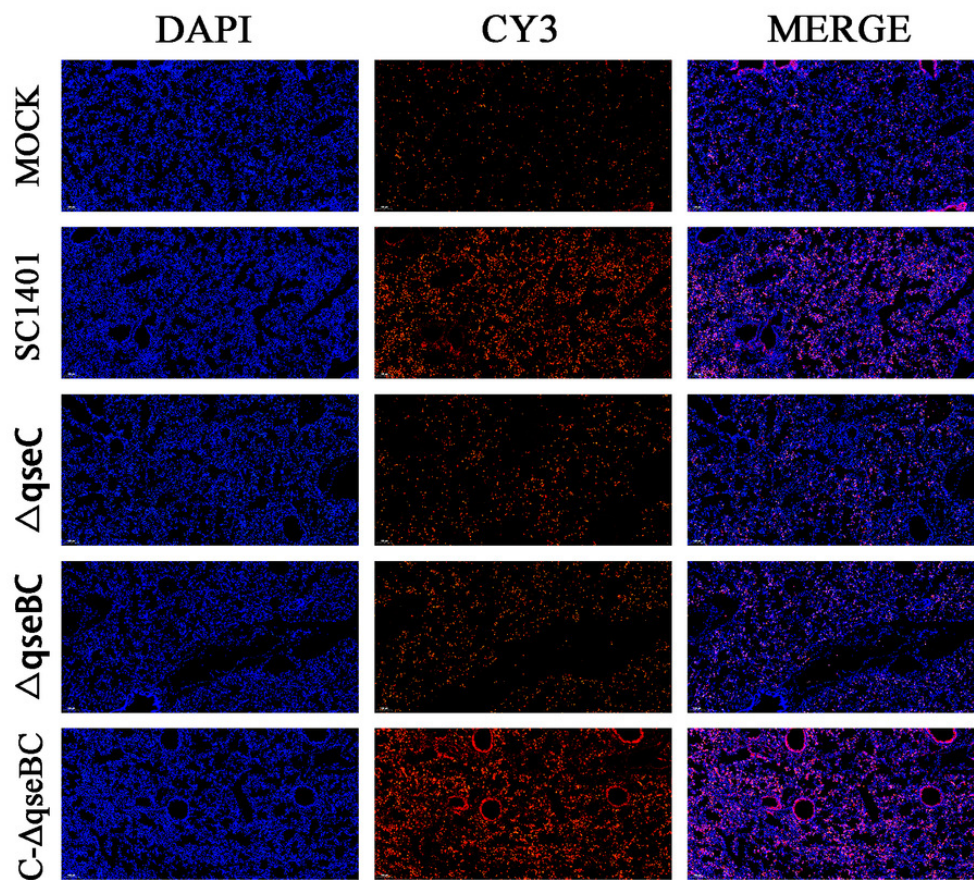
B

Figure 6

Apoptosis assay for the level of pathological les ion in lung tissues (TUNEL staining).

Lung tissues were harvested from mice in different groups after 4 dpi and used for FFPE treatment, pathological slice preparation, and IF assay for apoptosis. (**A**) IF analysis (100×). (**B**) Statistical analysis of IOD of myeloid cells (Biomarker: mpo) in mice lungs. Relative values of IOD_R were calculated by the ratio of the IOD of FITC-fluorescence intensity (IOD_F) and DAPI (IOD_D).

A

	DAPI	FITC	MERGE

MOCK

SC1401

ΔqseC

ΔqseBC

C-ΔqseBC

B
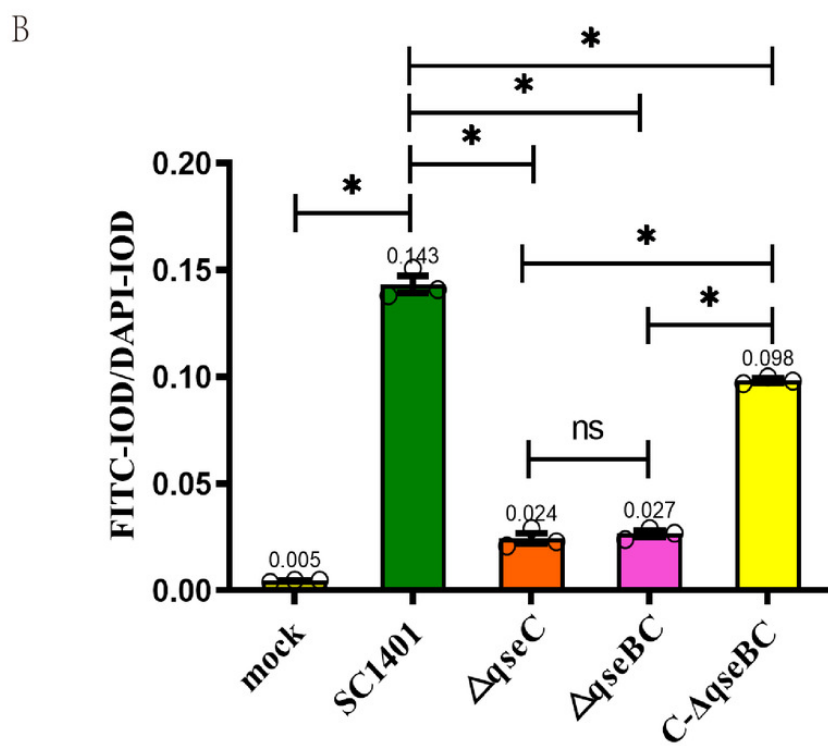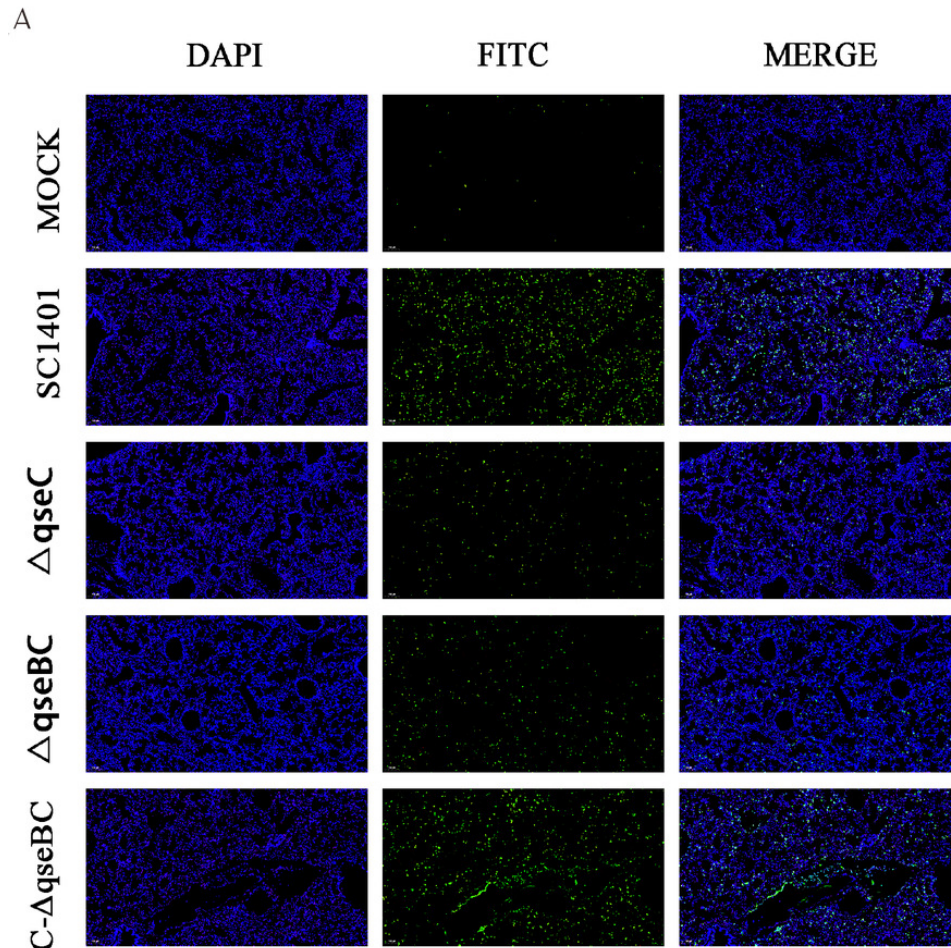
Bacteria strains and plasmids used in this study.

1 **Table 1** Bacteria strains and plasmids used in this study.

Strain or plasmid	Relevant characteristic(s)	Source
G. parasuis strains		
SC1401	Wild type, serovar 11 clinical isolate	Laboratory collection
△*qseBC*	SC1401 △*qseBC*::KanR	This study
C-△*qseBC*	SC1401 complemented △*qseBC* strain, Gm^R Kan^R	This study
E. coli strains		
E. coli DH5α	Cloning host for maintaining the recombinant plasmids	Laboratory collection
E. coli BL21	Expressing host for maintaining the recombinant plasmids	Laboratory collection
plasmids		
pMD19-T	T-vector, Amp^R	Takara
pET-28a	Expression vector, Kan^R	Laboratory collection
pET-32a	Expression vector, Amp^R	Laboratory collection
pk18mobsacB	Suicide and narrow-broad-host vector, Kan^R	Laboratory collection
pLQ4	A 2840-bp fragment containing Kan^R, the upstream sequences of *qseB* gene and downstream sequences of *qseC* gene in	This study

	pK18mobsacB, Kan^R	
PLQ5	A 2056-bp fragment containing Gm^R and the *qseBC* gene in PSF116	This study
PSF116	Gm resistance cassette-carrying vector, Gm^R	Zou et al.2016
pKD4	Amp^R, Kan^R, gene knock-out vector	Laboratory collection

2 Kan, kanamycin; Gm, gentamicin; R, resistence.

Primers used in this study.

1 **Table 2** Primers used in this study.

Primer name	Sequence (5'-3')
For construction of mutant and complementary strain	
P1(*qseBC*-Up-F)	ctatgacatgattacgaattcACCGCTTGTAGCTACCCCTGAAGGCTTTAAAC
P2(*qseBC*-Up-R)	GCAGGGCTTCCCAACCTTACCTCAACCTCCCAATTTCAAAAAAG
P3(*qseBC*-Down-F)	**G**GGGTTCGAAATGACCGACCAGGATGGAGATATAAGGCACAAAC
P4(*qseBC*-Down-R)	caggtcgactctagaggatccACCGCTTGTCCGTCTTTAGTGATGGTTGGTG
P5(*qseBC*-Comp-F)	gaagtttctatgtaaggtaccAGATTACTGTTGATATTGATGACGAGG
P6(*qseBC*-Comp-R)	gcttatgtcaattcgggatcc TCAGGACGGAGTTTGACGGC
P7(*Kan*-F)	GTAAGGTTGGGAAGCCCTGCAAAGT
P8(*Kan*-R)	GGTCGGTCATTTCGAACCCCAGAGT
P9(*qseBC*-F)	ATGCGTATTTTATTAGTTGAAGACG
P10(*qseBC*-R)	TCAGGACGGAGTTTGACGGCAC
P11(HPS-F)	GTGATGAGGAAGGGTGGTGT
P12(HPS-R)	GGCTTCGTCACCCTCTGT
P13(*qseB*-F)	CGGGATCCATGCGTATTTTATTAATTGAAG

P14(*qseB*-R)	CCCAAGCTTTTAAGCAACTTCATCGTTTTTTC
P15(*qseC*-F)	CGGGATCCATGAAGTTGCTTAAAAATACC
P16(*qseC*-R)	CCCAAGCTTTCAGGACGGAGTTTGACGGC
P17(*qseBC*(200)-F)	AGATTACTGTTGATATTGATGACGAGG
P18(*qseBC*(200)-R)	CGTATTGCTCATTTTACCAAGTCAA
For RT-qPCR	
P19 A4U84_RS03675-F	GCGATTACTCCAGCAAGCCA
P20 A4U84_RS03675-R	ATCTCACCGCTTGCATCACG
P21 *groES*-F	GGCCATTGCCAACAGCAATC
P22 *groES*-R	TCGTCCGTTACACGACAAAGT
P23 16SrRNA-F	CCACCTGCCATAAGATGAGC
P24 16SrRNA-R	GGACCGTGTCTCAGTTCCAG